J. Fluid Mech. (2023), *vol*. 956, A12, doi:10.1017/jfm.2022.1094

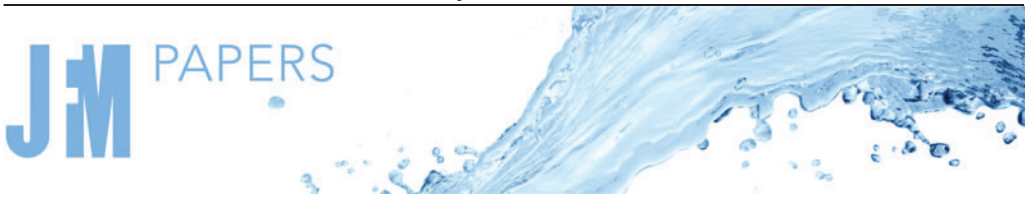

Selective energy and enstrophy modification of two-dimensional decaying turbulence

Aditya G. Nair[1],†, **James Hanna**[1] **and Matteo Aureli**[1]

[1]Department of Mechanical Engineering, University of Nevada, Reno, NV 89557, USA

(Received 29 July 2021; revised 14 October 2022; accepted 12 December 2022)

In two-dimensional decaying homogeneous isotropic turbulence, kinetic energy and enstrophy are respectively transferred to larger and smaller scales. In such spatiotemporally complex dynamics, it is challenging to identify the important flow structures that govern this behaviour. We propose and employ numerically two flow-modification strategies that leverage the inviscid global conservation of energy and enstrophy to design external forcing inputs that change these quantities selectively and simultaneously, and drive the system towards steady-state or other late-stage behaviour. One strategy employs only local flow field information, while the other is global. We observe various flow structures excited by these inputs and compare them with recent literature. Energy modification is characterized by the excitation of smaller wavenumber structures in the flow than enstrophy modification.

Key words: isotropic turbulence

1. Introduction

Turbulent flows exhibit nonlinear interactions over a wide range of spatiotemporal scales. In two-dimensional (2-D) decaying turbulence, the rate of energy dissipation is slowed considerably by kinetic energy transfer to large-scale coherent vortex cores through the inverse energy flux mechanism (Kraichnan 1967; McWilliams 1990; Bracco *et al.* 2000; Fox & Davidson 2010; Boffetta & Ecke 2012), while the enstrophy dissipation rate is enhanced by enstrophy transfer to small-scale eddies (Weiss 1991). The identification and modification of collective structures in the flow that accelerate or decelerate the inverse energy flux mechanism or alter the enstrophy cascade is a fundamental question (Hunt, Wray & Moin 1988; Holmes *et al.* 2012). This is unlikely to be addressed by flow-modification strategies based on linearization of the Navier–Stokes equations and reduced-order/surrogate representations that lack strict adherence to conservation laws.

† Email address for correspondence: adityan@unr.edu

The objective of the current work is to tie a flow-modification strategy directly to the governing equations and their ensuing conservation laws.

A comparison of the behaviour of decaying 2-D turbulence with either well-developed vortices or phase-scrambled initial conditions revealed the crucial role of coherent vortex structures in suppressing the cascade rate (McWilliams 1990). More recent studies by Jiménez (2020*a*,*b*) have shed light on the connections between dipoles (counter-rotating vortices) and streams (formed by the concatenation of dipoles) on the kinetic energy of the flow. These findings have been corroborated by network-theoretic approaches using induced velocity and flow perturbations (Yeh, Meena & Taira 2021). However, these recent data-intensive approaches require either machine learning to extract templates of dynamical significance or some explicit knowledge of vortical interactions in the flow. In the present work, we provide explicit physical definitions of forcing terms to be added to the Navier–Stokes equations, capable of altering conserved quantities independently, and revealing automatically the flow structures of significance.

Several previous efforts have focused on the exclusive modification of single conserved quantities in fluid flows. Vallis, Carnevale & Young (1989) and Shepherd (1990) modified the Euler equations to alter energy while preserving topological invariants associated with the vorticity field. This enabled the discovery of isolated energy extrema and stable steady equilibria. Sadourny & Basdevant (1985) designed, and Vallis & Hua (1988) later employed, a subgrid-scale closure scheme that dissipates enstrophy while preserving energy. Another approach was developed by Gay-Balmaz & Holm (2013) and applied to dissipate the squared helicity while preserving energy in three-dimensional incompressible flow. A relevant early work with a more general context is that of Morrison (1986). Our approach is inspired by the recently introduced framework of exterior dissipation (Aureli & Hanna 2021; Hanna 2021), which enables proportional selective modification of multiple conserved quantities. We present local and global flow-modification approaches with three objectives: (i) to alter selectively and simultaneously any integral conserved quantities; (ii) to identify characteristic flow structures that accelerate or decelerate the inverse energy flux and enstrophy cascade; (iii) to discover and approach efficiently stable steady or slowly-varying states. In certain limits, our local approach leads to behaviour similar to that of Vallis *et al.* (1989) or Sadourny & Basdevant (1985).

2. Approach

We consider the 2-D flow of homogenous and incompressible fluid within a fixed bi-periodic square domain $\mathcal{D}$. The governing dynamics is given by the forced Navier–Stokes equations

$$\frac{\partial \boldsymbol{u}}{\partial t} = \underbrace{-\boldsymbol{u}\cdot\boldsymbol{\nabla}\boldsymbol{u} - \boldsymbol{\nabla}p/\rho}_{e_{\boldsymbol{u}}} + \underbrace{\nu\,\boldsymbol{\nabla}^2\boldsymbol{u}}_{d_{\boldsymbol{u}}} + \boldsymbol{f}_{\boldsymbol{u}}, \quad \boldsymbol{\nabla}\cdot\boldsymbol{u} = \boldsymbol{0}, \tag{2.1}$$

where $\boldsymbol{u} = \boldsymbol{u}(\boldsymbol{x}, t)$ is the velocity, p is the pressure, ρ is the density, ν is the kinematic viscosity, and $\boldsymbol{f}_{\boldsymbol{u}}$ is the external forcing to be designed. In the inviscid, unforced case, the flow admits the integral quadratic invariants Q_i of kinetic energy E and enstrophy Ω, defined as

$$Q_1 \equiv E = \int_{\mathcal{D}} \frac{1}{2}\,\boldsymbol{u}\cdot\boldsymbol{u}\,\mathrm{d}\boldsymbol{x}, \quad Q_2 \equiv \Omega = \int_{\mathcal{D}} \frac{1}{2}\,\boldsymbol{\omega}\cdot\boldsymbol{\omega}\,\mathrm{d}\boldsymbol{x}, \tag{2.2a,b}$$

where $\boldsymbol{\omega} = \boldsymbol{\nabla} \times \boldsymbol{u} = \omega \hat{\boldsymbol{k}}$ is the vorticity field. We may express the time derivatives of these conserved quantities as

$$\frac{\mathrm{d}}{\mathrm{d}t} Q_i = \int_{\mathcal{D}} \boldsymbol{b}_i \cdot \frac{\partial \boldsymbol{u}}{\partial t} \,\mathrm{d}\boldsymbol{x} = \int_{\mathcal{D}} \boldsymbol{b}_i \cdot \boldsymbol{e}_{\boldsymbol{u}} \,\mathrm{d}\boldsymbol{x} + \int_{\mathcal{D}} \boldsymbol{b}_i \cdot \boldsymbol{d}_{\boldsymbol{u}} \,\mathrm{d}\boldsymbol{x} + \int_{\mathcal{D}} \boldsymbol{b}_i \cdot \boldsymbol{f}_{\boldsymbol{u}} \,\mathrm{d}\boldsymbol{x}. \tag{2.3}$$

The contribution of the Euler term in (2.3) vanishes (Hasegawa 1985; Foias *et al.* 2001), i.e. $\int_{\mathcal{D}} \boldsymbol{b}_i \cdot \boldsymbol{e}_{\boldsymbol{u}} \,\mathrm{d}\boldsymbol{x} = 0$. The evolutions of kinetic energy and enstrophy are governed by $\boldsymbol{b}_1 = \boldsymbol{u}$ and $\boldsymbol{b}_2 = \boldsymbol{\nabla} \times \boldsymbol{\omega}$, respectively; using a vector calculus identity, $\boldsymbol{\omega} \cdot \boldsymbol{\omega} = \boldsymbol{\omega} \cdot \boldsymbol{\nabla} \times \boldsymbol{u} = \boldsymbol{u} \cdot (\boldsymbol{\nabla} \times \boldsymbol{\omega}) + \boldsymbol{\nabla} \cdot (\boldsymbol{u} \times \boldsymbol{\omega})$, but due to the bi-periodic boundary conditions, the divergence term vanishes, and we have simply

$$\int_{\mathcal{D}} \boldsymbol{\omega} \cdot \boldsymbol{\omega} \,\mathrm{d}\boldsymbol{x} = \int_{\mathcal{D}} \boldsymbol{u} \cdot (\boldsymbol{\nabla} \times \boldsymbol{\omega}) \,\mathrm{d}\boldsymbol{x}. \tag{2.4}$$

Along with (2.1), we also consider the forced vorticity transport equation in the form

$$\frac{\partial \omega}{\partial t} = \underbrace{\frac{\partial \omega}{\partial y}\frac{\partial \psi}{\partial x} - \frac{\partial \omega}{\partial x}\frac{\partial \psi}{\partial y}}_{J(\omega,\psi)} + \underbrace{\nu \nabla^2 \omega}_{d_\omega} + f_\omega, \tag{2.5}$$

where $\boldsymbol{u} = \boldsymbol{\nabla} \times (\psi \hat{\boldsymbol{k}})$ defines the streamfunction ψ, and f_ω is the external forcing to be designed. The integral kinetic energy and enstrophy invariants (Boffetta & Ecke 2012) and their time derivatives may be expressed as

$$Q_1 \equiv E = \int_{\mathcal{D}} \frac{1}{2}\,\omega\psi \,\mathrm{d}\boldsymbol{x}, \quad Q_2 \equiv \Omega = \int_{\mathcal{D}} \frac{1}{2}\,\omega^2 \,\mathrm{d}\boldsymbol{x}, \quad \frac{\mathrm{d}}{\mathrm{d}t} Q_i = \int_{\mathcal{D}} b_i \frac{\partial \omega}{\partial t} \,\mathrm{d}\boldsymbol{x}, \tag{2.6a–c}$$

where the energy has been rewritten by eliminating a divergence term due to the bi-periodic boundary conditions. Similarly to before, $\int_{\mathcal{D}} b_i J(\omega, \psi) \,\mathrm{d}\boldsymbol{x} = 0$. Note that the b_i in (2.6*a–c*) are distinct from the $\boldsymbol{b}_i$ in (2.3). We find that $b_1 = \psi$, by a manipulation of

$$\frac{\partial}{\partial t} \int_{\mathcal{D}} \left(\frac{1}{2}\,\boldsymbol{u} \cdot \boldsymbol{u} \right) \mathrm{d}\boldsymbol{x} = \int_{\mathcal{D}} \boldsymbol{\nabla} \times (\psi \hat{\boldsymbol{k}}) \cdot \frac{\partial \boldsymbol{u}}{\partial t} \,\mathrm{d}\boldsymbol{x} \tag{2.7}$$

and elimination of a divergence term, while clearly $b_2 = \omega$.

The vector and scalar equations (2.1) and (2.5) will be the respective starting points for local and global approaches to systematically modify the inviscid conservation or viscous non-conservation of the integral quantities Q_i. Each approach generates a unique forcing term, as described below.

2.1. *Local formulation*

We first construct an external forcing term $\boldsymbol{f}_{\boldsymbol{u}} = \boldsymbol{f}_{\boldsymbol{u}}(\boldsymbol{x}, t)$ in (2.1) using only local flow field information. Inspired by Hanna (2021) and Aureli & Hanna (2021), we define

$$\boldsymbol{f}_{\boldsymbol{u}} = -\epsilon_1 (\boldsymbol{b}_1 \wedge \boldsymbol{b}_2) \cdot \boldsymbol{b}_2 - \epsilon_2 (\boldsymbol{b}_2 \wedge \boldsymbol{b}_1) \cdot \boldsymbol{b}_1, \tag{2.8}$$

where $\boldsymbol{b}_1 = \boldsymbol{u}$ and $\boldsymbol{b}_2 = (\boldsymbol{\nabla} \times \boldsymbol{\omega})$ as discussed above, and ϵ_1 and ϵ_2 are constant coefficients. The wedge product $\wedge$ of two vectors in three dimensions is

$2\boldsymbol{b}_1 \wedge \boldsymbol{b}_2 = \boldsymbol{b}_1\boldsymbol{b}_2 - \boldsymbol{b}_2\boldsymbol{b}_1$, where juxtaposition indicates the standard tensor product. The terms in (2.8) can be rearranged into double cross-products:

$$\boldsymbol{f}_{\boldsymbol{u}} = -\frac{\epsilon_1}{2}\underbrace{\left(\|\nabla\times\boldsymbol{\omega}\|^2\,\boldsymbol{u} - [\boldsymbol{u}\cdot(\nabla\times\boldsymbol{\omega})]\,\nabla\times\boldsymbol{\omega}\right)}_{\boldsymbol{b}_2\times(\boldsymbol{b}_1\times\boldsymbol{b}_2)} - \frac{\epsilon_2}{2}\underbrace{\left(\|\boldsymbol{u}\|^2\,\nabla\times\boldsymbol{\omega} - [\boldsymbol{u}\cdot(\nabla\times\boldsymbol{\omega})]\,\boldsymbol{u}\right)}_{\boldsymbol{b}_1\times(\boldsymbol{b}_2\times\boldsymbol{b}_1)}. \quad (2.9)$$

The first term exclusively alters the integral flow energy, while the second exclusively alters the integral flow enstrophy, allowing for independent manipulation of these two quantities. (The construction of $\boldsymbol{b}_2$ involved the discarding of a divergence term. Thus the first term in $\boldsymbol{f}_{\boldsymbol{u}}$ does actually change the local vorticity magnitude and enstrophy, but its effect is a pure divergence that does not affect the global conservation.) If $\epsilon_1 = 0$, then energy is conserved, while enstrophy is increased (decreased) if $\epsilon_2 < 0$ ($\epsilon_2 > 0$). Similarly, if $\epsilon_2 = 0$, then enstrophy is conserved, while energy is increased (decreased) if $\epsilon_1 < 0$ ($\epsilon_1 > 0$). In what follows, $\epsilon_2 \geq 0$.

In the inviscid case, the rates of change of the integrals Q_i can be rearranged into the simple forms

$$\int_{\mathcal{D}} \boldsymbol{b}_i \cdot \boldsymbol{f}_{\boldsymbol{u}}\,\mathrm{d}\boldsymbol{x} = -\frac{\epsilon_i}{2}\int_{\mathcal{D}}\left[\boldsymbol{u}\times(\nabla\times\boldsymbol{\omega})\right]^2\mathrm{d}\boldsymbol{x} = -\frac{\epsilon_i}{2}\int_{\mathcal{D}}[\boldsymbol{u}\cdot\nabla\boldsymbol{\omega}]^2\,\mathrm{d}\boldsymbol{x}, \quad (2.10)$$

where we have used the fact that $\int_{\mathcal{D}}(\nabla\boldsymbol{\omega})\cdot\boldsymbol{u}\,\mathrm{d}\boldsymbol{x}$ vanishes for 2-D flow. These two rates are proportional, thus the quantity $E/\epsilon_1 - \Omega/\epsilon_2$ is conserved (Hanna 2021), which seems to ensure that the resulting dynamics are not simply driven to a trivial equilibrium when both quantities are dissipated. The rates vanish when the two $\boldsymbol{b}_i$ align. Remarkably, when $\epsilon_2 = 0$, the rate of change of energy is the same as that generated by the method of Vallis *et al.* (1989), and when $\epsilon_1 = 0$, the rate of change of enstrophy is the same as that generated by the method of Sadourny & Basdevant (1985).

2.2. *Global formulation*

We next construct an alternative external forcing term $f_\omega = f_\omega(\boldsymbol{x}, t)$ in (2.5) incorporating global flow field information. Interpreting the integrals of (2.6*a–c*) as inner products of square-integrable functions on $\mathcal{D}$ allows for a formal analogy with the framework of Aureli & Hanna (2021), in which scalar fields are now regarded as infinite-dimensional vectors. We mimic the algebraic construction of exterior dissipation in Aureli & Hanna (2021) by introducing an array $\boldsymbol{B} = (b_1, b_2) = (\psi, \omega)$ produced by stacking the vectors b_i, and the Gram matrix $\boldsymbol{G}$ of the inner products of b_1 and b_2,

$$\boldsymbol{G} = \int_{\mathcal{D}}\begin{bmatrix}\psi^2 & \psi\omega\\ \psi\omega & \omega^2\end{bmatrix}\mathrm{d}\boldsymbol{x}. \quad (2.11)$$

The global forcing is constructed as

$$f_\omega = -\tfrac{1}{2}\,\boldsymbol{B}\,\mathrm{adj}(\boldsymbol{G})\,\boldsymbol{\epsilon}, \quad (2.12)$$

where $\mathrm{adj}(\cdot)$ denotes the adjugate (transpose of the cofactor matrix), and $\boldsymbol{\epsilon} = (\epsilon_1, \epsilon_2)$ is an array containing the constant coefficients exclusively modulating the rates of E and Ω,

respectively. Explicitly,

$$f_\omega = -\frac{\epsilon_1}{2}\left(\psi\int_{\mathcal{D}}\omega^2\,\mathrm{d}\boldsymbol{x} - \omega\int_{\mathcal{D}}\psi\omega\,\mathrm{d}\boldsymbol{x}\right) - \frac{\epsilon_2}{2}\left(\omega\int_{\mathcal{D}}\psi^2\,\mathrm{d}\boldsymbol{x} - \psi\int_{\mathcal{D}}\psi\omega\,\mathrm{d}\boldsymbol{x}\right). \quad (2.13)$$

In the inviscid case, the rates of change of the integrals Q_i are

$$\int_{\mathcal{D}} b_i f_\omega\,\mathrm{d}\boldsymbol{x} = -\frac{\epsilon_i}{2}\left(\int_{\mathcal{D}}\psi^2\,\mathrm{d}\boldsymbol{x}\int_{\mathcal{D}}\omega^2\,\mathrm{d}\boldsymbol{x}\right)\sin^2(\beta), \quad (2.14)$$

where β indicates the 'angle' between the vectors b_i in the function space, defined by $\cos\beta = \int_{\mathcal{D}}\psi\omega\,\mathrm{d}\boldsymbol{x}/\sqrt{\int_{\mathcal{D}}\psi^2\,\mathrm{d}\boldsymbol{x}\int_{\mathcal{D}}\omega^2\,\mathrm{d}\boldsymbol{x}}$. As before, the rates are proportional, vanishing when $\beta = 0$ (when ψ and ω 'align'), and again the quantity $E/\epsilon_1 - \Omega/\epsilon_2$ is conserved.

2.3. *Viscous compensation*

Both external forcing and viscosity break the invariance of conserved quantities. The forcing terms offer a means to compensate for viscous decay of energy and enstrophy, through the augmentation of the constant coefficients ϵ_i by additional time-varying coefficients ϵ_i^ν that can eliminate the effect of viscosity on these quantities or set their rates to some other desired behaviour. The rates of change of the conserved quantities with viscous compensation are

$$\frac{\mathrm{d}}{\mathrm{d}t}Q_i = D_i - \epsilon_i^\nu F \quad \Rightarrow \quad \epsilon_i^\nu = \frac{1}{F}\left(D_i - \frac{\mathrm{d}}{\mathrm{d}t}Q_i\right), \quad (2.15)$$

where $D_i \equiv \int_{\mathcal{D}} \boldsymbol{b}_i \cdot \boldsymbol{d}_{\boldsymbol{u}}\,\mathrm{d}\boldsymbol{x}$ and $F \equiv -(1/\epsilon_i)\int_{\mathcal{D}} \boldsymbol{b}_i \cdot \boldsymbol{f}_{\boldsymbol{u}}\,\mathrm{d}\boldsymbol{x}$ for the local formulation ((2.3) and (2.10)), while $D_i \equiv \int_{\mathcal{D}} b_i d_\omega\,\mathrm{d}\boldsymbol{x}$ and $F \equiv -(1/\epsilon_i)\int_{\mathcal{D}} b_i f_\omega\,\mathrm{d}\boldsymbol{x}$ for the global formulation ((2.6*a–c*) and (2.14)). Note that F does not carry a subscript as it is the same for both quantities. As this shared forced rate F tends to zero, compensation becomes impractical, requiring large coefficients ϵ_i^ν.

2.4. *Numerical set-up*

Two-dimensional direct numerical simulations are performed using a Fourier spectral method and a fourth-order Runge–Kutta time integration scheme on a square bi-periodic computational domain of sides $L = 1$ with 1024×1024 grid points in the x- and y-directions. Further details of the set-up can be found in Taira, Nair & Brunton (2016). The definitions of spatial and temporal scales, along with their initial values, are shown in table 1. The initial values are indicated with a subscript 0. The spatial scales are normalized by the initial integral length scale l_0, and the time scales are normalized by the initial large-eddy turnover time τ_0. The isotropic energy spectrum for 2-D turbulence is defined as $E(k) = \pi k\langle|\hat{\boldsymbol{u}}(\boldsymbol{k})|^2\rangle$ (where the average $\langle\cdot\rangle$ is over all $|\boldsymbol{k}| = k$) and $\hat{\boldsymbol{u}}(\boldsymbol{k}) = \int_{\mathcal{D}} \boldsymbol{u}(\boldsymbol{x})\,\mathrm{e}^{\mathrm{i}\boldsymbol{k}\cdot\boldsymbol{x}}\,\mathrm{d}\boldsymbol{x}$ (Boffetta & Ecke 2012). All the simulations are performed such that $k_{max}\eta \geq 8$, with k_{max} the maximum resolvable wavenumber, and η the smallest (Kolmogorov) length scale. The initial Reynolds number based on the integral length scale for all the viscous simulations is fixed at $Re_0 \approx 713.1780$.

The initial condition for all the simulations is shown in figure 1(*a*). We also show corresponding energy spectra $E(k)$, and dissipation (scaled enstrophy) spectra $2\nu\,\Omega(k)$, with $\Omega(k) = k^2\,E(k)$, as the unforced flow evolves. We can see the presence of the classical

Variable	Definition	Initial value
r.m.s. velocity	$u^* = \sqrt{\frac{1}{L^2}\int_{\mathcal{D}} \boldsymbol{u}\cdot\boldsymbol{u}\,\mathrm{d}\boldsymbol{x}}$	$u_0^* = 0.7587$
r.m.s. vorticity	$\omega^* = \sqrt{\frac{1}{L^2}\int_{\mathcal{D}} \boldsymbol{\omega}\cdot\boldsymbol{\omega}\,\mathrm{d}\boldsymbol{x}}$	$\omega_0^* = 16.1564$
Integral length scale	$l = u^*/\omega^*$	$l_0 = 0.0470$
Reynolds number	$Re = u^* l/\nu$	$Re_0 = 713.1780$
Eddy turnover time	$\tau = l/u^*$	$\tau_0 = 0.0619$
Small (Kolmogorov) scale	$\eta \sim l\,Re^{-1/2}$	$\eta_0 \sim 0.0018$

Table 1. Flow field parameters ($L = 1$).

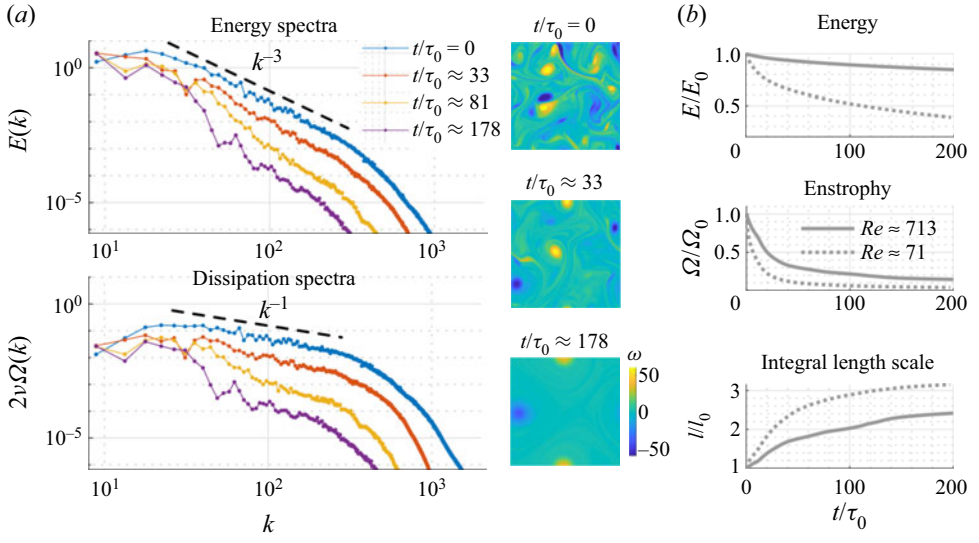

Figure 1. Baseline (unforced) 2-D decaying homogeneous isotropic turbulent flow: (*a*) spectral evolution of energy and enstrophy, with plots of vorticity fields; (*b*) time history of energy, enstrophy and integral length scale for two different initial Reynolds numbers.

k^{-3} turbulent energy spectra and k^{-1} dissipation spectra at the initial condition of the turbulent flow, and the breakdown of the scaling leading to the eventual formation of large coherent structures. The evolution of energy E, enstrophy Ω, and integral length scale l for two different Reynolds numbers over a long time period $0 \leq t/\tau_0 \leq 200$ is shown in figure 1(*b*). The rates of decay of energy (in particular) and enstrophy decrease with increasing Re.

In the following section, we present and discuss the implications of local and global modification of inviscid, viscous, and compensated viscous flows. We define $\delta_1 \equiv \epsilon_1 F_0/E_0$ and $\delta_2 \equiv \epsilon_2 F_0/\Omega_0$ as normalized rates at which energy and enstrophy, respectively, are injected (negative) or extracted (positive). For the local formulation, the maximum resolvable wavenumber limits the maximum rates of modification.

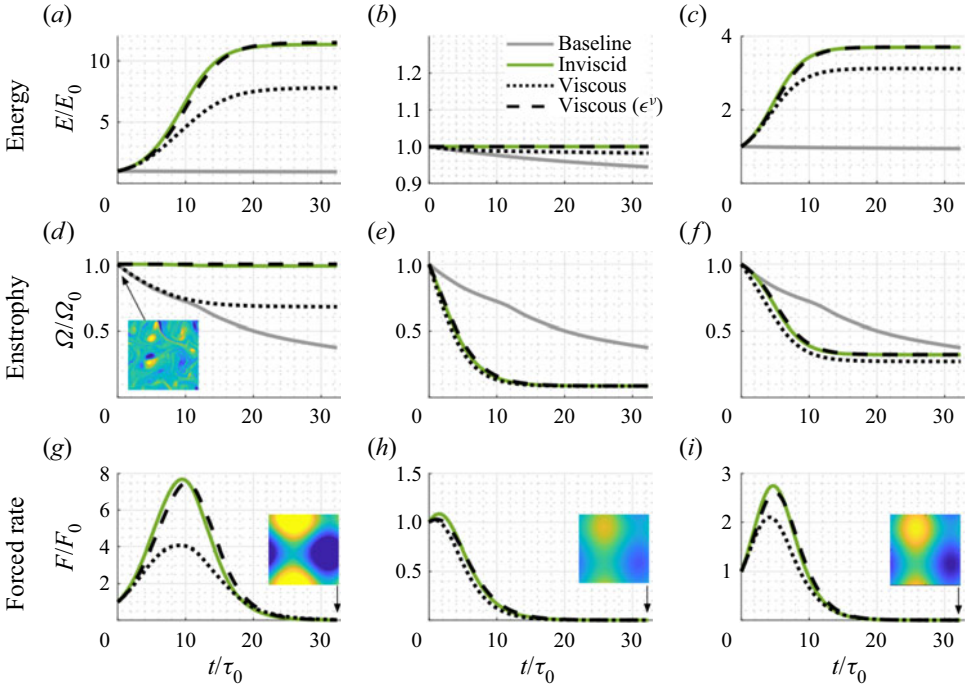

Figure 2. Trajectories of energy, enstrophy and the shared forced rate of change of these quantities for global forcing of 2-D turbulent flow: (*a*,*d*,*g*) modification of energy, $\delta_1 = -1$, $\delta_2 = 0$; (*b*,*e*,*h*) modification of enstrophy, $\delta_1 = 0$, $\delta_2 = 1$; (*c*,*f*,*i*) modification of both quantities, $\delta_1 = -1$, $\delta_2 = 0.25$. The unforced viscous baseline simulation is shown in grey, the modified inviscid flow in green, viscous flows in black dotted, and compensated viscous flows in black dashed. Also shown in (*g*,*h*,*i*) (insets) are late-stage ($t/\tau_0 \approx 33$) vorticity snapshots for the globally modified viscous flows.

3. Results and discussion

The effects of global forcing are shown in figure 2. The evolution of energy, enstrophy and the shared forced rate of change of these quantities F is shown over the time window $0 \leq t/\tau_0 \leq 33$ for the unforced viscous baseline simulation (grey) and for the modified inviscid (green), viscous (black dotted) and compensated viscous (black dashed) flows. Three modification cases are shown: forced energy injection, $\delta_1 = -1$, $\delta_2 = 0$ (figures 2*a*,*d*,*g*); forced enstrophy dissipation, $\delta_1 = 0$, $\delta_2 = 1$ (figures 2*b*,*e*,*h*); and simultaneous forcing to inject energy and dissipate enstrophy, $\delta_1 = -1$, $\delta_2 = 0.25$ (figures 2*c*,*f*,*i*). Compensated viscous flows have an additional time-dependent modification to fully cancel the additional energy and enstrophy decay induced by viscous dissipation. The trajectories of these simulations are similar to those of the inviscid cases, although not identical, as the forcing is being applied to a different flow, albeit one with the same energy and enstrophy as the inviscid flow.

The maximum energy reached in figures 2(*a*,*d*,*g*) is higher for the inviscid flow than the viscous flow. The enstrophy is invariant in the inviscid setting, while for the viscous case, the enstrophy initially decays at the same rate as the baseline but quickly saturates to a nearly-constant value around $t/\tau_0 > 10$. At this time, the forcing term F reaches a peak and subsequently drops to zero as the system approaches a late-stage slowly decaying nearly steady state after $t/\tau_0 > 25$. Late-stage vorticity snapshots for the globally modified viscous flows are also shown. The inverse cascade in decaying turbulence leads

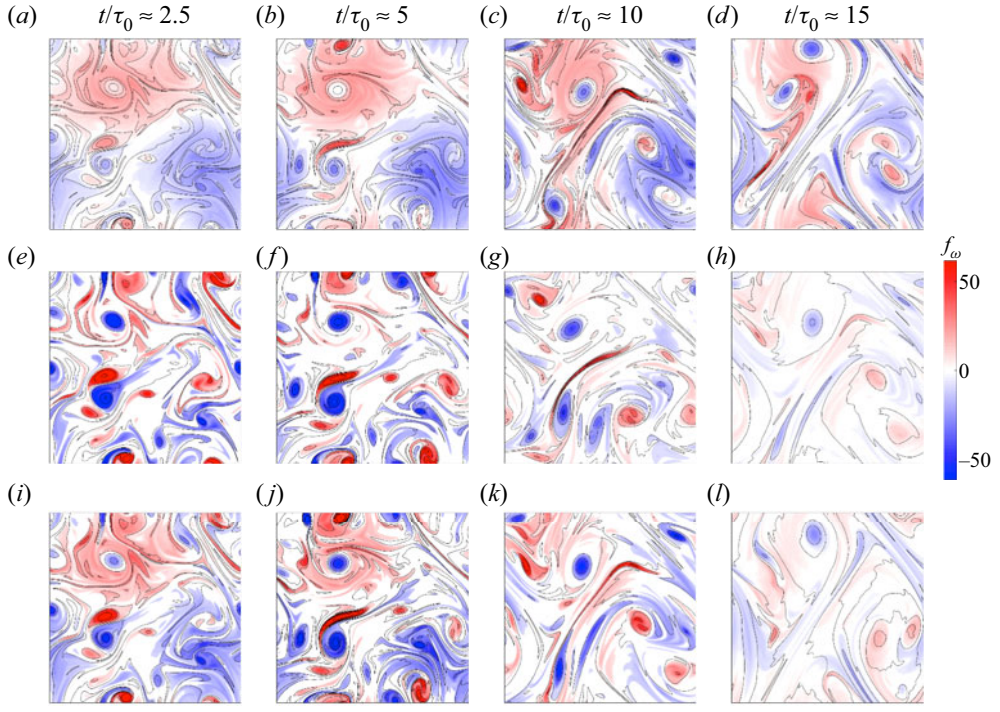

Figure 3. Forcing fields f_ω superimposed on vorticity contours (black) for global forcing of 2-D turbulent flow: (*a–d*) modification of energy, $\delta_1 = -1$, $\delta_2 = 0$; (*e–h*) modification of enstrophy, $\delta_1 = 0$, $\delta_2 = 1$; (*i–l*) modification of both quantities, $\delta_1 = -1$, $\delta_2 = 0.25$.

to the formation of a dipole (Smith & Yakhot 1993). The formation of this structure is accelerated with energy and enstrophy modification. The minimum enstrophy achieved in figures 2(*b*,*e*,*h*) is nearly identical for the inviscid and viscous flows, with a nearly-steady state reached quickly around $t/\tau_0 > 10$. The mixed case in figures 2(*c*,*f*,*i*) shares a combination of the features observed in figures 2(*a*,*d*,*g*) and 2(*b*,*e*,*h*).

Shown in figure 3 is the global forcing f_ω at several times, superimposed on vorticity contours. We observe that energy modification excites streams (fast regions between vortex dipoles) and some other more diffuse regions between vortex cores, while enstrophy modification excites vortex cores. This is consistent with the conclusions from Jiménez (2020*a*) and McWilliams (1990), where streams and vortex cores were found to be the relevant structures correlated with energy and enstrophy, respectively. As the solution approaches the late-stage flow, the forcing inputs fade, and indeed vanish in the inviscid case. All of the forced cases approach a non-trivial steady or slowly-varying state with a characteristic length scale of the order of the system size.

For the energy modification and enstrophy modification cases, we compare the global forcing f_ω with the enstrophy field and a scalar measure of the strain field in figures 4(*a–c*) and 4(*d–f*), respectively, at $t/\tau_0 \approx 10$. The enstrophy field $\boldsymbol{\omega}^2$ can be computed easily from the vorticity. For 2-D incompressible flow, an appropriate invariant measure of strain (Weiss 1991; Oetzel & Vallis 1997) is the determinant of (twice) the symmetric part of the

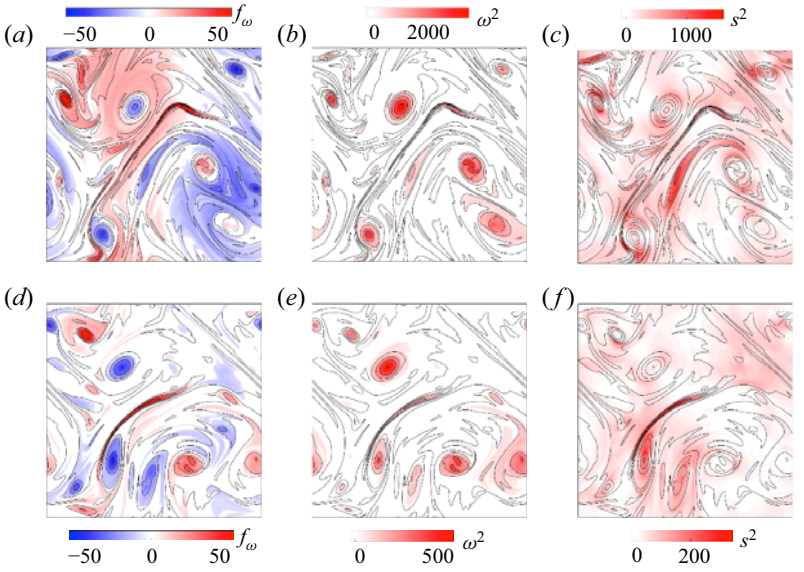

Figure 4. (*a*,*d*) The forcing field f_ω, (*b*,*e*) the enstrophy field $\boldsymbol{\omega}^2$, and (*c*,*f*) the strain field s^2, superimposed on vorticity contours (black) at $t/\tau_0 \approx 10$ for (*a*–*c*) modification of energy, $\delta_1 = -1$, $\delta_2 = 0$, and (*d*–*f*) modification of enstrophy, $\delta_1 = 0$, $\delta_2 = 1$.

velocity gradient tensor $\boldsymbol{\Sigma}$, given by

$$\boldsymbol{\Sigma} = \begin{bmatrix} \dfrac{\partial u}{\partial x} & \dfrac{\partial u}{\partial y} \\ \dfrac{\partial v}{\partial x} & \dfrac{\partial v}{\partial y} \end{bmatrix}. \tag{3.1}$$

We employ $s^2 \equiv -\det(\boldsymbol{\Sigma} + \boldsymbol{\Sigma}^{\mathrm{T}})$. The energy forcing operates both in regions of significant strain and vorticity, while the enstrophy forcing is, not surprisingly, more strongly associated with the latter. It is clear that the forcing fields are distinct from either of the two measures.

To quantify the influence of the rate parameters δ_1 and δ_2 on the system trajectories, we run additional simulations for energy and enstrophy modification as shown in figures 5(*a*,*c*,*e*) and 5(*b*,*d*,*f*), respectively. For energy modification, we can see that late-stage energy saturates at different values for different forcing δ_1. However, for enstrophy modification, the enstrophy trajectories saturate to the same level. This is also evident in the values of velocity and vorticity magnitude of late-stage flow fields at $t/\tau_0 = 30$ in table 2. The integral length scale at this late stage is nearly identical for all modified cases. As seen in table 2, the mixed case leads to lower values of vorticity and velocity than the purely energy-modified case.

We also show the viscous decay rate $D_i = \int_{\mathcal{D}} b_i d_\omega \, \mathrm{d}\boldsymbol{x}$ for energy and enstrophy modification in figures 5(*c*,*d*). We see that for the baseline flow, the viscous energy decay rate decreases monotonically, while the viscous enstrophy rate initially decreases, then increases to a peak value around $t/\tau_0 = 26$, and subsequently decreases again. For cases with $\delta_2 \geq 0.5$, the non-monotonic behaviour in the decay rate disappears. The viscous enstrophy decay rate for the baseline flow follows $[\Omega/\log(l/\eta)]^p$, where $p = 3/2$ (Davidson 2015). For the modified flows, we find empirically $p = 1.66$, 2.42 and 3.00 for

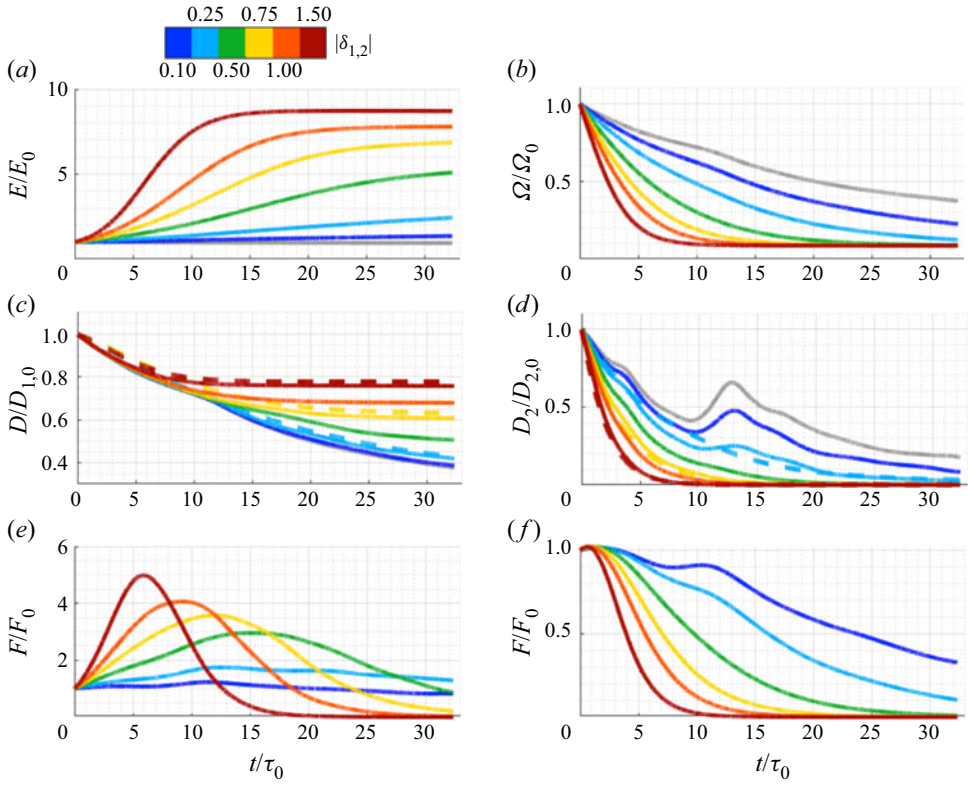

Figure 5. Influence of rate parameters (δ_1 and δ_2) on global forcing of 2-D turbulent flow: (*a*,*c*,*e*) modification of energy, and (*b*,*d*,*f*) modification of enstrophy. Trajectories of energy/enstrophy, viscous decay rate, and the forced rates of change of these quantities are shown. The unforced viscous baseline simulation is in grey. The dashed lines in (*c*,*d*) are empirical fits to scaling laws, discussed in the text.

Case	δ_1	δ_2	u^*/u_0^*	ω^*/ω_0^*	l/l_0
Baseline	0	0	0.97	0.61	1.59
Energy forcing	−0.75	0	2.61	0.78	3.35
	−1	0	2.79	0.82	3.40
	−1.5	0	2.95	0.87	3.39
Enstrophy forcing	0	0.75	0.99	0.29	3.41
	0	1	0.99	0.29	3.41
	0	1.5	0.99	0.29	3.41
Combined forcing	−1	0.25	1.76	0.52	3.38

Table 2. Values at $t/\tau_0 \approx 30$.

$\delta_2 = 0.25$, 0.5 and 0.75, respectively. As shown by the dashed lines, the viscous energy decay rate for modified flows follows $[E/\log(l/\eta)]^q$, where $q = -1.0$, -0.24 and -0.12 for $\delta_1 = 0.5$, 0.75 and 1.5, respectively. The forced rates for various cases are shown in figures 5(*e*,*f*). For the cases with $\delta_1 \leq 0.25$, viscous dissipation effects dominate the

external energy forcing input, and correspondingly the flow does not show large changes in energy. For $\delta_1 \geq 0.5$, a peak in the shared forced rate is observed. The times corresponding to the peaks decrease with increasing δ_1, reflecting a more rapid approach to late-stage behaviour.

In decaying turbulence, energy accumulates in the smallest wavenumber $k_{min} \approx 1/L$, leading to condensate formation (Boffetta & Ecke 2012). The formation of the condensate is accelerated with the modification of energy and enstrophy. We show the centroid wavenumbers of the energy spectra $k_c(E)$ and enstrophy spectra $k_c(\Omega)$ for the energy and enstrophy modified cases in figures 6(*a*) and 6(*b*), respectively. Here, $k_c(E) = \int_0^{k_{max}} k\,E(k)\,\mathrm{d}k / \int_0^{k_{max}} E(k)\,\mathrm{d}k$ and $k_c(\Omega) = \int_0^{k_{max}} k\,\Omega(k)\,\mathrm{d}k / \int_0^{k_{max}} \Omega(k)\,\mathrm{d}k$. As the flow evolves, the baseline flow centroid energy and enstrophy wavenumbers both decrease non-monotonically (McWilliams 1990). This non-monotonicity is suppressed for modified flows with $\delta_2 \geq 0.5$.

We show the spectrogram of energy and enstrophy for baseline flow in figures 6(*c*) and 6(*d*), respectively, and for the modified energy with $\delta_1 = -1$ in figure 6(*e*) and modified enstrophy with $\delta_2 = 1$ in figure 6(*f*). (Slices through figures 6(*e*,*f*) can be seen in figures 6(*i*,*j*).) We can see here the distribution of energy in the range of wavenumbers $k \approx 10$–50 and the distribution of enstrophy in the range $k \approx 50$–150. Both the centroid plots and spectrograms show rapid shifts towards low wavenumbers for the modified energy and enstrophy. We also show the transfer of energy $T_E(k,t) = \partial E(k)/\partial t + 2\nu k^2 E(k)$ and enstrophy $T_\Omega(k,t) = \partial \Omega(k)/\partial t + 2\nu k^2 \Omega(k)$ in figures 6(*g*) and 6(*h*) for the respective modified cases. There is a large positive transfer of energy to smaller wavenumbers for energy modification throughout the entire time period considered, while for enstrophy modification, the transfers die out fairly quickly.

To illustrate further these effects of the modification in the physical domain, we compute the 2-D signature function $V(r) = \int_0^{k_{max}} E(k)\,\mathrm{J}_3(kr)\,k\,\mathrm{d}k$, where J_3 is a Bessel function of the first kind. This function represents the measure of energy held in eddies of size r, and is related to the second-order structure function of the flow (Davidson 2015). The signature function for the baseline flow is shown in figure 7(*a*). The energy modification cases with $\delta_1 = -0.5$ and -1 are shown in figures 7(*b*) and 7(*c*), respectively. The enstrophy modification cases with $\delta_2 = 0.5$ and $\delta_2 = 1$ are shown in figures 7(*d*) and 7(*e*), respectively. Initially, much of the energy in the baseline flow is concentrated near the initial integral length scale $r \approx l_0$. As the modified flows evolve, energy gets distributed across eddies of different sizes, with a shift towards larger sizes. As the energy of the flow increases for energy-modified cases, we see a larger magnitude associated with the signature function. The energy is unaffected by forcing in the enstrophy modification cases, so the corresponding energy level decreases, as in the baseline flow.

The effects of local forcing are shown in figures 8 and 9, and compared with the global forcing in figure 8. The evolution of energy, enstrophy and the integral length scale is shown over the time window $0 \leq t/\tau_0 \leq 33$ for the unforced viscous baseline simulation (grey) and for the locally (magenta or orange) and globally (black) modified viscous (dotted) and compensated viscous (dashed) flows. Three modification cases are shown: forced energy injection $\delta_1 = -0.1$, $\delta_2 = 0$, magenta, or dissipation $\delta_1 = 0.1$, $\delta_2 = 0$, orange (figures 8*a*,*d*,*g*), forced enstrophy dissipation $\delta_1 = 0$, $\delta_2 = 0.1$ (figures 8*b*,*e*,*h*), and simultaneous forcing to inject energy and dissipate enstrophy $\delta_1 = 0.1$, $\delta_2 = 0.25$ (figures 8*c*,*f*,*i*). Here, the compensated viscous flows are designed so that the viscous contribution to the decay of energy and enstrophy matches that of the unforced baseline flow. The forcing coefficients are smaller than those used in figure 2 because the achievable

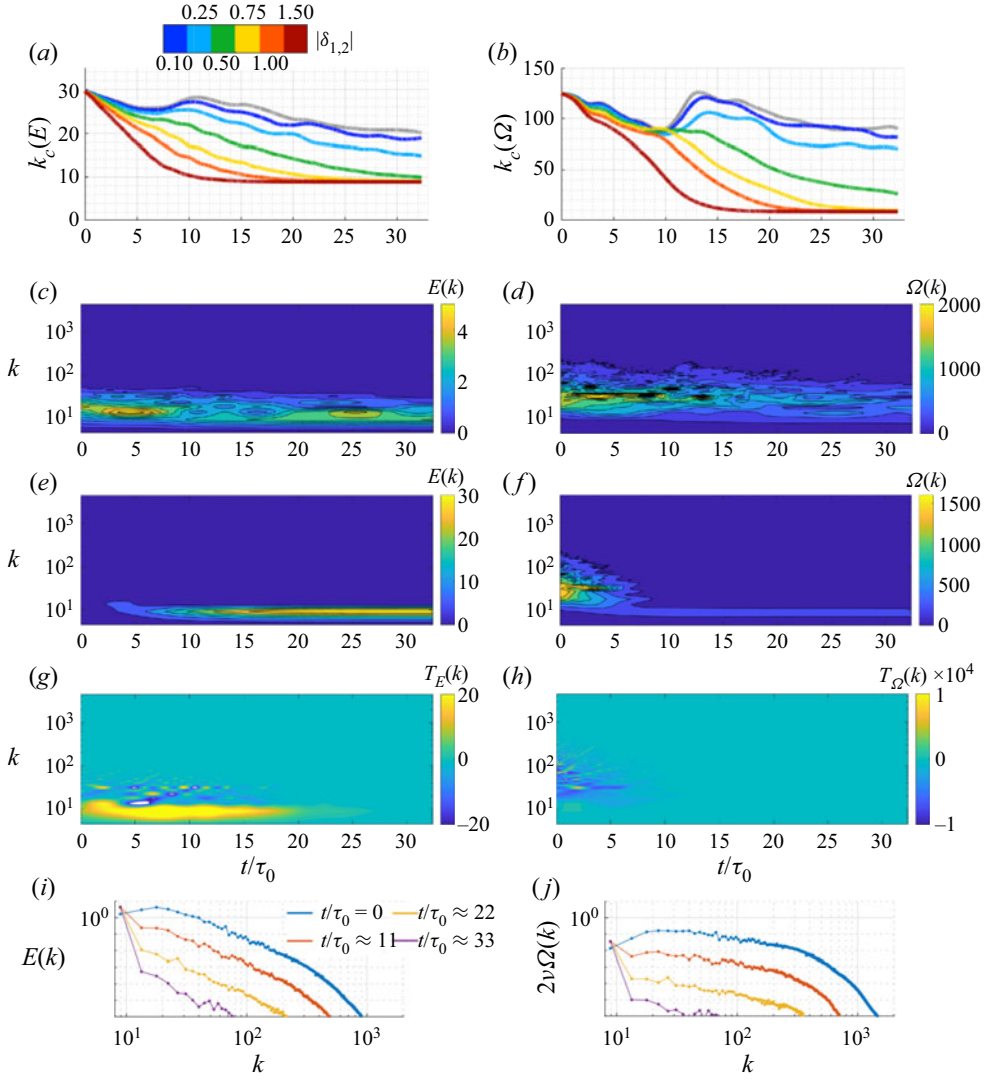

Figure 6. Influence of rate parameters (δ_1 and δ_2) on spectra for global forcing of 2-D turbulent flow. Centroid wavenumbers of (*a*) energy and (*b*) enstrophy spectra, with the unforced viscous baseline in grey. Baseline flow spectrograms of (*c*) energy and (*d*) enstrophy. Spectrograms of (*e*) energy and (*g*) energy transfer in the energy-modified case $\delta_1 = -1$, and (*f*) enstrophy and (*h*) enstrophy transfer in the enstrophy-modified case $\delta_2 = 1$. Spectral evolution for (*i*) the energy-modified case $\delta_1 = -1$, and (*j*) the enstrophy-modified case $\delta_2 = 1$.

rate of local forcing is limited by the maximum resolvable wavenumber. Therefore, the systems do not approach late-stage behaviour in this time window.

We find that the global forcing is significantly more effective than the local forcing in changing the quantities of interest. In particular, the effect of the local modification on enstrophy in figures 8(*e*) and 8(*f*) is weak. The behaviour of the integral length scales is curious. Note that the integral length scale is simply the square root of the ratio of energy to enstrophy. As shown earlier, in figure 1, lower Reynolds number baseline flows are characterized by faster decay of both energy and enstrophy, and more rapid growth of

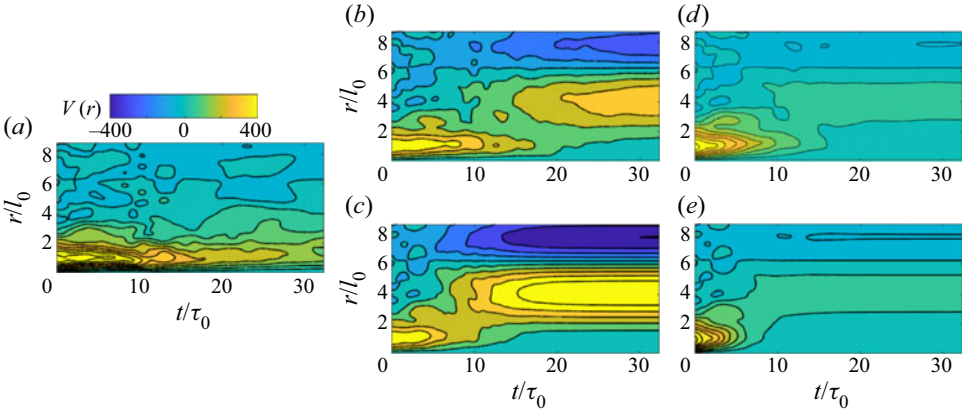

Figure 7. Two-dimensional signature function $V(r)$ (see text) for (a) baseline, energy modification with (b) $\delta_1 = -0.5$ and (c) $\delta_1 = -1$, and enstrophy modification with (d) $\delta_2 = 0.5$ and (e) $\delta_2 = 1$.

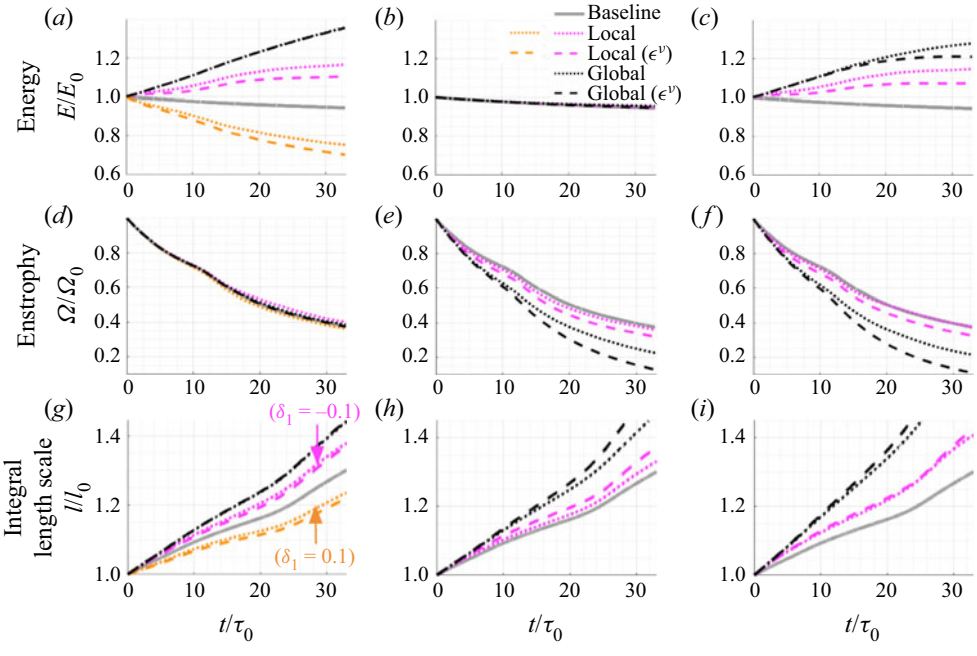

Figure 8. Comparison of local and global forcing of 2-D turbulent flow: (a,d,g) modification of energy, $\delta_1 = -0.1$, $\delta_2 = 0$ (magenta), $\delta_1 = 0.1$, $\delta_2 = 0$ (orange); (b,e,h) modification of enstrophy, $\delta_1 = 0$, $\delta_2 = 0.1$; (c,f,i) modification of both quantities, $\delta_1 = -0.1$, $\delta_2 = 0.1$. Trajectories of energy, enstrophy and the integral length scale are shown for the unforced viscous baseline simulation (grey) and for the the locally (magenta or orange) and globally (black) modified viscous (dotted) and compensated viscous (dashed) flows.

integral length scale. Yet figures 8(a,d,g) show that when we decrease (orange) or increase (magenta) the energy through forcing, this decelerates or accelerates, respectively, the growth of the integral length scale.

Figure 9 shows the local forcing $(\boldsymbol{\nabla} \times \boldsymbol{f_u}) \cdot \hat{\boldsymbol{k}}$ at several times for the locally modified viscous flows with energy injection and/or enstrophy dissipation. These local forcing fields are significantly different from the global ones in figure 3. Energy modification

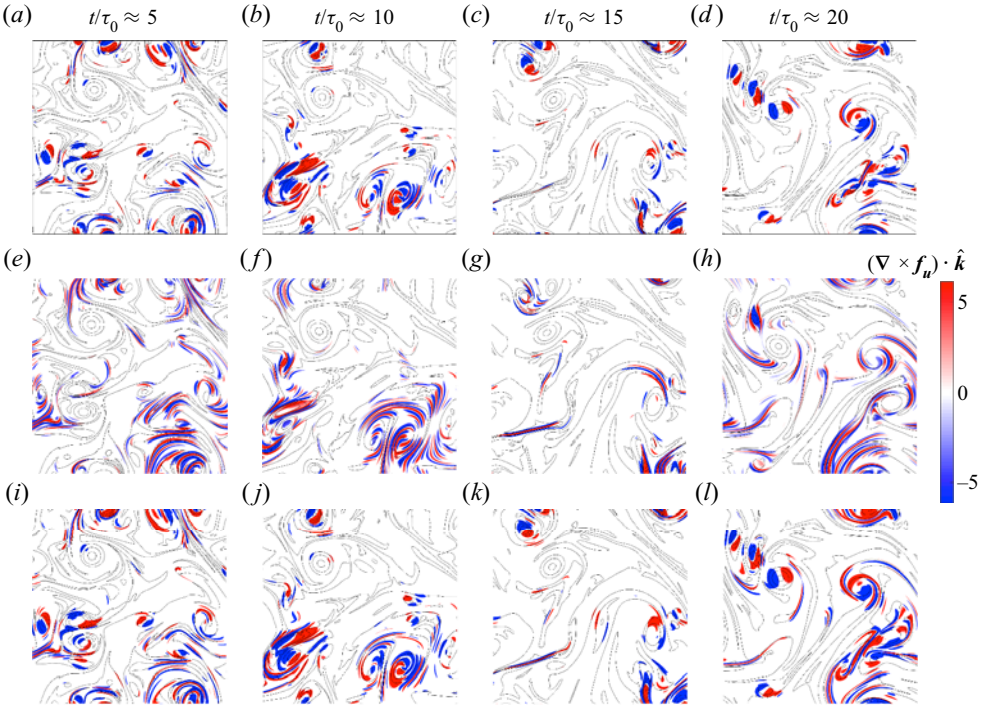

Figure 9. Forcing fields $(\nabla \times \boldsymbol{f_u}) \cdot \hat{\boldsymbol{k}}$ superimposed on vorticity contours (black) for local forcing of 2-D turbulent flow: (*a–d*) modification of energy, $\delta_1 = -0.1$, $\delta_2 = 0$; (*e–h*) modification of enstrophy, $\delta_1 = 0$, $\delta_2 = 0.1$; (*i–l*) modification of both quantities, $\delta_1 = -0.1$, $\delta_2 = 0.1$.

introduces new dipolar structures near existing vortex cores, while enstrophy modification introduces streaky elongated dipolar structures between the cores. These streaks help the filamentation process of vorticity, accelerating the enstrophy cascade (Davidson 2015). The latter is reminiscent of recent findings using broadcast mode analysis (Yeh *et al.* 2021), where streaks occupying low-vorticity regions were found to be the most sensitive structures to flow perturbations. The forcings have spectra $E_f(k) = \pi k \langle |\hat{\boldsymbol{f}}_{\boldsymbol{u}}(\boldsymbol{k})|^2 \rangle$ (where the average $\langle \cdot \rangle$ is over all $|\boldsymbol{k}| = k$) and $\Omega_f(k) = k^2 E_f(k)$, shown in figure 10 for the two pure cases. They evolve non-monotonically. These modifications are characterized by wavenumbers k below $\approx$100 and above $\approx$100 for enstrophy. This difference reflects the simultaneous acceleration of the inverse energy and enstrophy fluxes to larger and smaller scales, respectively.

Figure 11 shows the influence of local energy and enstrophy modification on the spectral statistics of the flow. In particular, we show the centroid energy and enstrophy wavenumbers in figures 11(*a*,*b*), similar to figures 6(*a*,*b*). We also show the centroid wavenumbers of the forcing fields for energy- and enstrophy-modified cases. We see that for $\delta_1 = -0.1$, the energy transfers to smaller wavenumbers compared to the baseline, resulting in acceleration of the inverse energy flux, while for $\delta = 0.1$, energy transfers to higher wavenumbers compared to the baseline, slowing down the inverse flux cascade. For the enstrophy modification, we see that although initially the centroid wavenumbers are identical, the enstrophy transfers to lower wavenumbers than the baseline. The corresponding centroid of the wavenumbers of energy forcing lies in the range $50 \leq k_c(E_f) \leq 120$ (corresponding to the elongated dipoles), while the centroid of the

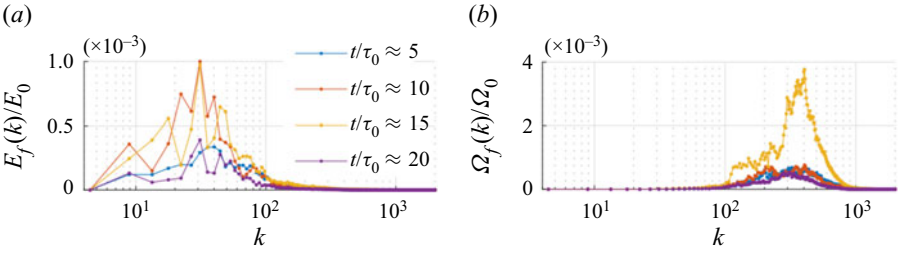

Figure 10. Spectra (arbitrary units) corresponding only to the forcing-induced velocity in locally modified viscous flows at several times: (*a*) forced energy spectrum from modification of energy, $\delta_1 = -0.1$, $\delta_2 = 0$; (*b*) forced enstrophy spectrum from modification of enstrophy, $\delta_1 = 0$, $\delta_2 = 0.1$.

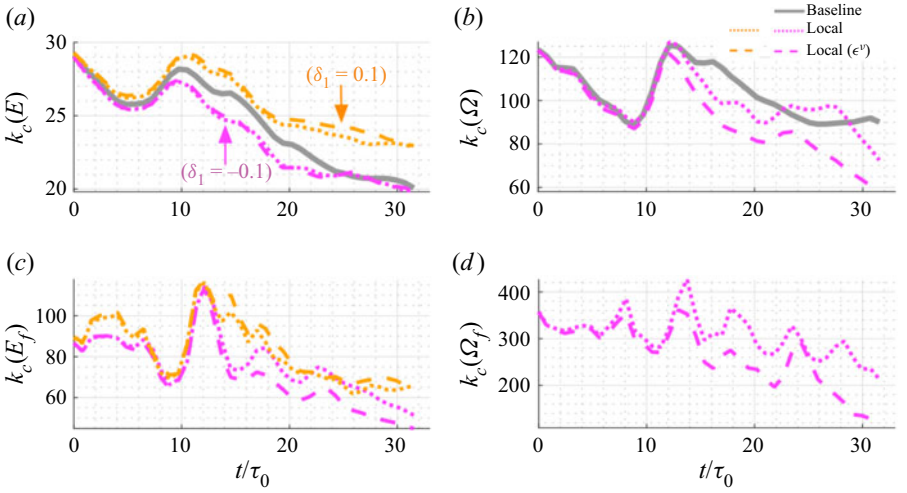

Figure 11. Centroid wavenumbers for: (*a*,*c*) modification of energy, $\delta_1 = -0.1$, $\delta_2 = 0$ (magenta), $\delta_1 = 0.1$, $\delta_2 = 0$ (orange); (*b*,*d*) modification of enstrophy, $\delta_1 = 0$, $\delta_2 = 0.1$. (*a*,*b*) Centroid energy and enstrophy centroid wavenumbers of the flow; (*c*,*d*) corresponding centroid wavenumbers of the forcing. The modified viscous and compensated viscous flow trajectories are shown with dotted and dashed lines, with the unforced viscous baseline in grey.

wavenumbers of enstrophy forcing lies in the range $200 \leq k_c(E_f) \leq 400$, corresponding to the elongated streaks.

4. Conclusions and future directions

We have introduced local and global flow-modification strategies that selectively modulate energy and enstrophy in 2-D decaying homogeneous isotropic turbulence. Acceleration or deceleration of large-scale coherent vortex core formation is achievable. Through their selective excitation, these two strategies reveal and/or excite different flow structures that have been observed previously and obtained through disparate means. For the global flow-modification strategy, the late-stage vorticity saturates at different levels for different energy forcing rates, while it saturates at the same level for the enstrophy forcing rates considered. The late-stage integral length scales achieved are similar for all the modified cases. The enstrophy forcing is associated with vortex cores for the global strategy, while it introduces streaky elongated dipolar structures for the local strategy. For negative rates of

the local energy forcing, the energy transfers to smaller wavenumbers as compared to the baseline flow, accelerating the inverse energy flux, while for positive rates, the energy transfers to higher wavenumbers as compared to the baseline flow, slowing down the inverse flux cascade. Modification of energy or enstrophy is associated with the excitation of lower and higher wavenumbers, respectively.

One issue with which we did not concern ourselves is to what extent our modifications violate the conservation of integral linear and angular momentum. However, it would be straightforward to include any number of additional quantities within the framework of Aureli & Hanna (2021). Another significant omission is the role of (wall) boundaries, which might be better addressed from a Lagrangian point of view. Extensions of the present Eulerian approach to forced and three-dimensional turbulence are currently underway. The latter replaces enstrophy with helicity and allows for changes in vorticity without changes in enstrophy, and one may expect that selectively decreasing energy will Beltramize the flow (Vallis *et al.* 1989). Another possibility is to use these flow modifications to construct closure schemes for modelling of turbulent flows (Sadourny & Basdevant 1985), such that the effects of higher wavenumbers on energy and other quantities are mimicked by the modification terms. The present work suggests a promising approach for closed-loop turbulence control.

Declaration of interests. The authors report no conflict of interest.

Author ORCIDs.
Aditya G. Nair https://orcid.org/0000-0002-8979-8420;
Matteo Aureli https://orcid.org/0000-0003-4242-0081.

Author contributions. All authors derived the theory together. A.G.N. guided the study, performed the simulations and analysed the data. A.G.N. and J.H. wrote the paper.

Data availability statement. The data and code that support the findings of this study will be openly available in github.com/nairaditya on publication.

References

Aureli, M. & Hanna, J.A. 2021 Exterior dissipation, proportional decay, and integrals of motion. *Phys. Rev. Lett.* **127**, 134101.

Boffetta, G. & Ecke, R.E. 2012 Two-dimensional turbulence. *Annu. Rev. Fluid Mech.* **44**, 427–451.

Bracco, A., McWilliams, J.C., Murante, G., Provenzale, A. & Weiss, J.B. 2000 Revisiting freely decaying two-dimensional turbulence at millennial resolution. *Phys. Fluids* **12** (11), 2931–2941.

Davidson, P.A. 2015 *Turbulence: An Introduction for Scientists and Engineers*. Oxford University Press.

Foias, C., Manley, O., Rosa, R. & Temam, R. 2001 *Navier–Stokes Equations and Turbulence*. Cambridge University Press.

Fox, S. & Davidson, P.A. 2010 Freely decaying two-dimensional turbulence. *J. Fluid Mech.* **659**, 351.

Gay-Balmaz, F. & Holm, D.D. 2013 Selective decay by Casimir dissipation in inviscid fluids. *Nonlinearity* **26** (2), 495.

Hanna, J.A. 2021 An integrable family of torqued, damped, rigid rotors. *Mech. Res. Commun.* **116**, 103768.

Hasegawa, A. 1985 Self-organization processes in continuous media. *Adv. Phys.* **34** (1), 1–42.

Holmes, P., Lumley, J.L., Berkooz, G. & Rowley, C.W. 2012 *Turbulence, Coherent Structures, Dynamical Systems and Symmetry*. Cambridge University Press.

Hunt, J.C.R., Wray, A. & Moin, P. 1988 Eddies, stream, and convergence zones in turbulent flows. In *Center for Turbulence Research Report CTR-S88*, pp. 193–208.

Jiménez, J. 2020*a* Dipoles and streams in two-dimensional turbulence. *J. Fluid Mech.* **904**, A39.

Jiménez, J. 2020*b* Monte Carlo science. *J. Turbul.* **21** (9–10), 544–566.

Kraichnan, R.H. 1967 Inertial ranges in two-dimensional turbulence. *Phys. Fluids* **10** (7), 1417–1423.

McWilliams, J.C. 1990 A demonstration of the suppression of turbulent cascades by coherent vortices in two-dimensional turbulence. *Phys. Fluids* A **2** (4), 547–552.

MORRISON, P.J. 1986 A paradigm for joined Hamiltonian and dissipative systems. *Physica* D **18** (1–3), 410–419.

OETZEL, K.G. & VALLIS, G.K. 1997 Strain, vortices, and the enstrophy inertial range in two-dimensional turbulence. *Phys. Fluids* **9** (10), 2991–3004.

SADOURNY, R. & BASDEVANT, C. 1985 Parameterization of subgrid scale barotropic and baroclinic eddies in quasi-geostrophic models: anticipated potential vorticity method. *J. Atmos. Sci.* **42** (13), 1353–1363.

SHEPHERD, T.G. 1990 A general method for finding extremal states of Hamiltonian dynamical systems, with applications to perfect fluids. *J. Fluid Mech.* **213** (1), 573–587.

SMITH, L.M. & YAKHOT, V. 1993 Bose condensation and small-scale structure generation in a random force driven 2D turbulence. *Phys. Rev. Lett.* **71** (3), 352.

TAIRA, K., NAIR, A.G. & BRUNTON, S.L. 2016 Network structure of two-dimensional decaying isotropic turbulence. *J. Fluid Mech.* **795**, R2.

VALLIS, G.K., CARNEVALE, G.F. & YOUNG, W.R. 1989 Extremal energy properties and construction of stable solutions of the Euler equations. *J. Fluid Mech.* **207**, 133–152.

VALLIS, G.K. & HUA, B. 1988 Eddy viscosity of the anticipated potential vorticity method. *J. Atmos. Sci.* **45** (4), 617–627.

WEISS, J. 1991 The dynamics of enstrophy transfer in two-dimensional hydrodynamics. *Physica* D **48** (2–3), 273–294.

YEH, C., MEENA, M.G. & TAIRA, K. 2021 Network broadcast analysis and control of turbulent flows. *J. Fluid Mech.* **910**, A15.